ACS Catalysis

pubs.acs.org/acscatalysis

Research Article

Elucidating the Formation and Structural Evolution of Platinum Single-Site Catalysts for the Hydrogen Evolution Reaction

Peng Tang, Hyeon Jeong Lee, Kevin Hurlbutt, Po-Yuan Huang, Sudarshan Narayanan, Chenbo Wang, Diego Gianolio, Rosa Arrigo, Jun Chen, Jamie H. Warner, and Mauro Pasta*

Cite This: *ACS Catal.* 2022, 12, 3173−3180

Read Online

ACCESS | Metrics & More | Article Recommendations | Supporting Information

ABSTRACT: Platinum single-site catalysts (SSCs) are a promising technology for the production of hydrogen from clean energy sources. They have high activity and maximal platinum-atom utilization. However, the bonding environment of platinum during operation is poorly understood. In this work, we present a mechanistic study of platinum SSCs using operando, synchrotron-X-ray absorption spectroscopy. We synthesize an atomically dispersed platinum complex with aniline and chloride ligands onto graphene and characterize it with ex-situ electron microscopy, X-ray diffractometry, X-ray photoelectron spectroscopy, X-ray absorption near-edge structure spectroscopy (XANES), and extended X-ray absorption fine structure spectroscopy (EXAFS). Then, by operando EXAFS and XANES, we show that as a negatively biased potential is applied, the Pt−N bonds break first followed by the Pt−Cl bonds. The platinum is reduced from platinum(II) to metallic platinum(0) by the onset of the hydrogen-evolution reaction at 0 V. Furthermore, we observe an increase in Pt−Pt bonding, indicating the formation of platinum agglomerates. Together, these results indicate that while aniline is used to prepare platinum SSCs, the single-site complexes are decomposed and platinum agglomerates at operating potentials. This work is an important contribution to the understanding of the evolution of bonding environment in SSCs and provides some molecular insights into how platinum agglomeration causes the deactivation of SSCs over time.

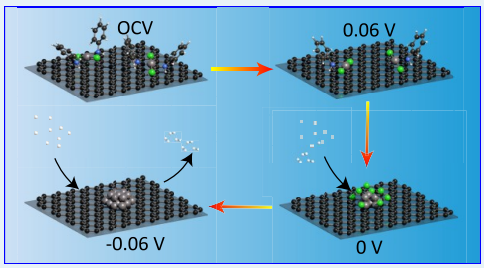

KEYWORDS: *hydrogen evolution reaction, platinum, single-site catalysts, agglomerates, operando X-ray absorption spectroscopy*

INTRODUCTION

Catalysts for the electrochemical hydrogen evolution reaction (HER) are desirable to produce hydrogen from clean sources like solar energy.[1,2] Platinum is among the most active HER catalysts known in acidic media.[3] Platinum is a heterogeneous catalyst with the HER occurring only on the metal surface.[4] This can be prohibitively inefficient because platinum is so rare and expensive.[5]

Single-site catalysts (SSCs) are an emerging type of heterogeneous catalysts in which isolated metal sites are supported on suitable substrates.[6,7] Each metal site is well separated from other metal atoms by a distance greater than the length of the metallic chemical bond.[8,9] Platinum SSCs can be prepared by synthesizing a platinum complex and adsorbing the whole complex to a suitable substrate.[10−12] They have extremely high atom utilization because every catalytic atom is exposed to the reactants and available for reaction.[13,14] We choose to distinguish these structures from single-atom catalysts (SACs), which have also been shown to promote a broad range of catalytic reactions,[15−17] since the Pt SSCs we investigate are complexes of several atoms surrounding the catalytically active metal atom.[18,19]

Despite the promise of platinum SSCs for the HER, the bonding environment of platinum in these devices before and during operation is poorly understood.[20−23] Establishing the structure−property relationship between the platinum bonding and the electrochemical performance of the catalyst is critically important to enabling design of tailored, high-performing platinum SSCs.[24,25] Furthermore, platinum SSCs for the HER have poor long-term stability, but the cause of their degradation is poorly understood.[26] Operando spectroscopy methods are a power tool to determine at the molecular level why these catalysts deactivate over time.[27−30]

In this work, we examine the model SSC system of a platinum complex with aniline and chloride ligands (*trans*-dianilinedichloroplatinum(II)) adsorbed onto graphene. Graphene is an excellent substrate because of its high electronic conductivity, chemical stability[31] and the good contrast it provides with platinum in electron microscopy.[32] At the same time, aniline is stabilized via adsorption onto graphene through $\pi-\pi$ stacking interactions with the molecule's aromatic ring.[10] Furthermore, aniline readily complexes with platinum, and the

Received: December 24, 2021
Revised: February 4, 2022
Published: February 23, 2022

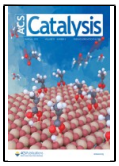

https://doi.org/10.1021/acscatal.1c05958
ACS Catal. 2022, 12, 3173−3180

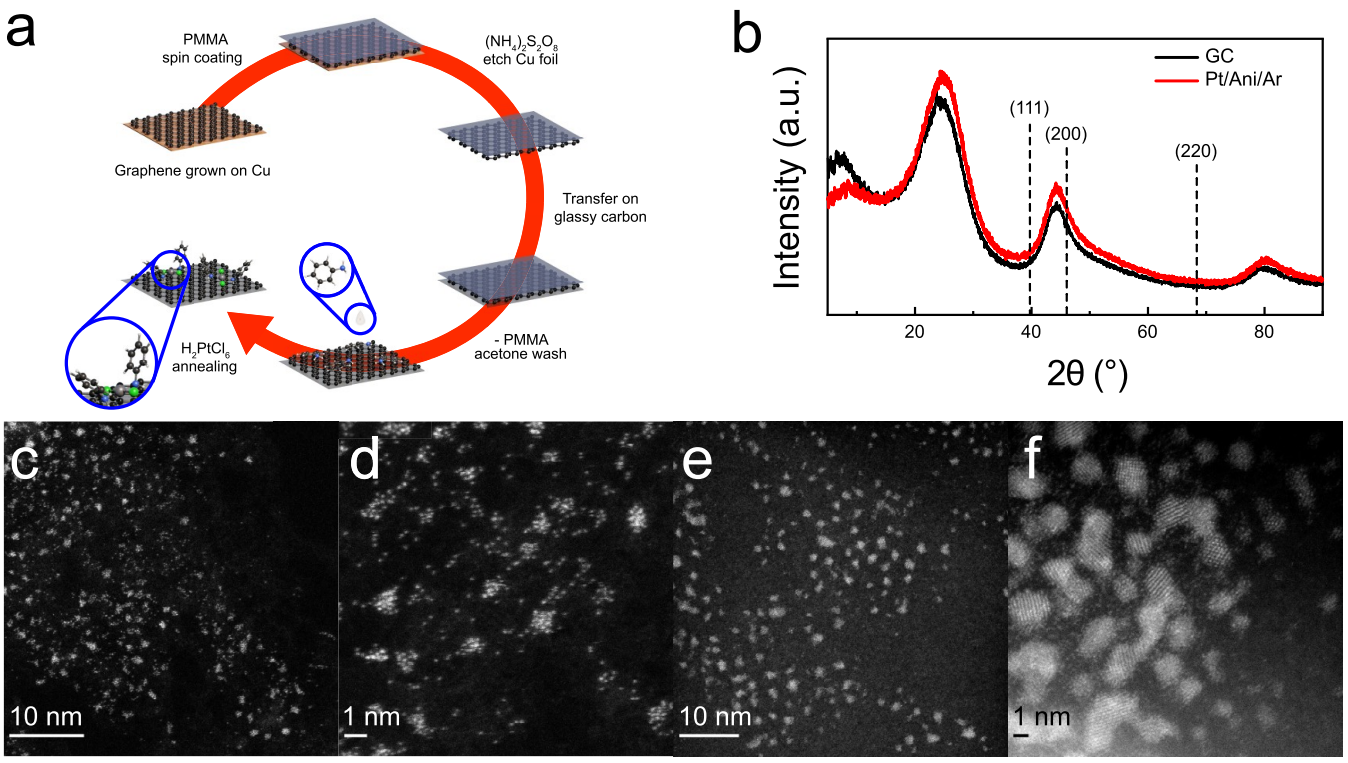

Figure 1. (a) Schematic illustration of the synthesis process (5 steps) for Pt SSC (gray, Pt; green, Cl; blue, N; black, carbon; white, H). Step 1: graphene nanosheets are grown by chemical vapor deposition (CVD) on copper. Step 2: copper foil is etched after spin coating with poly(methyl methacrylate) (PMMA) on top. Step 3: Thin-layer graphene coated with PMMA is then transferred onto a polished glassy carbon (GC) electrode. Step 4: after washing the PMMA with acetone and heating to 250 °C to remove trace organic contaminants, aniline is drop cast onto the graphene-coated GC electrode and dried. Step 5: chloroplatinic acid in ethanol is then drop cast and annealed under an argon atmosphere. This sample is referred to as the (Pt/Ani/Ar) sample. Control sample (Pt/Ar) is prepared by the same method but without aniline. (b) X-ray diffraction patterns for pristine GC and a (Pt/Ani/Ar) sample on GC; low-magnification to high-magnification atomic resolution HAADF-STEM images of (Pt/Ani/Ar) (c, d) and (Pt/Ar) (e, f).

molecule's large size provides a steric hindrance that can prevent platinum agglomeration.[33,34]

We characterize the physical structure of the as-synthesized SSC with ex-situ scanning transmission electron microscopy (STEM) and X-ray diffractometry (XRD). We examine the SSC's oxidation state and bonding environment with X-ray photoelectron spectroscopy (XPS), X-ray absorption near-edge structure spectroscopy (XANES), and extended X-ray absorption fine structure spectroscopy (EXAFS). Finally, we use chronoamperometry with operando EXAFS and XANES, fitted with structures calculated using density-functional theory (DFT), to study how platinum's bonding environment and coordination number change as a function of applied potential during the HER. This work is a good demonstration of using operando X-ray spectroscopy techniques to probe the atomic-level structural evolution of platinum SSCs for the HER during operation. This is an important contribution to the understanding of the synthesis and stability of platinum SSCs.

RESULTS AND DISCUSSION

Synthesis and Physicochemical Characterization. The platinum SSC is prepared according to a modified impregnation method described in detail in the Experimental Procedures section in the Supporting Information and outlined in Figure 1a.

High-angle annular dark-field scanning transmission electron microscopy (HAADF-STEM) of (Pt/Ani/Ar) and (Pt/Ar) are shown in Figure 1c and 1d and 1e and 1f, respectively. (Pt/Ani/Ar) contains atomically dispersed platinum with an average areal number density of about 0.5 nm^{-2} (Supplementary Figures S1 and S2). Some aggregates of platinum are present;[34] these are generally of size 1 nm or smaller (Supplementary Figure S2a). (Pt/Ar) mainly contains larger aggregates and nanoparticles that are up to about 4 nm across (Supplementary Figure S2b).

The XRD patterns for the glassy carbon (GC) electrode and for (Pt/Ani/Ar) are shown in Figure 1b.[35] The two patterns match well. In particular, the pattern for (Pt/Ani/Ar) lacks the intense peaks at about 39.8°, 46.2°, and 68.5° expected for the (111), (200), and (220) reflections in crystalline platinum (PDF# 04-0802). This implies that the HAADF-STEM images, which show no platinum nanoparticles in (Pt/Ani/Ar), are representative of the bulk sample. The STEM images show that treatment with aniline promotes the formation of more atomically dispersed platinum.

Ex-Situ XPS and XAS. The platinum oxidation state was investigated by XPS, and the spectra for (Pt/Ani/Ar) and (Pt/Ar) are shown in Figure 2a. Two standards are also shown: ammonium hexachloroplatinate(IV) ($(NH_4)_2PtCl_6$) and platinum(II) chloride ($PtCl_2$). The platinum $4f_{7/2}$ peak in $PtCl_2$ has a binding energy of 72.9 eV, consistent with the +2 oxidation state. The $(NH_4)_2PtCl_6$ has a higher binding energy of 75.2 eV, which is also expected for its high oxidation state of +4. The spectrum for (Pt/Ani/Ar) is well fitted by a 74% contribution from a peak centered at 72.8 ± 0.1 eV and a 26% contribution from a peak centered at 74.6 ± 0.1 eV (Figure 2a

https://doi.org/10.1021/acscatal.1c05958
ACS Catal. 2022, 12, 3173−3180

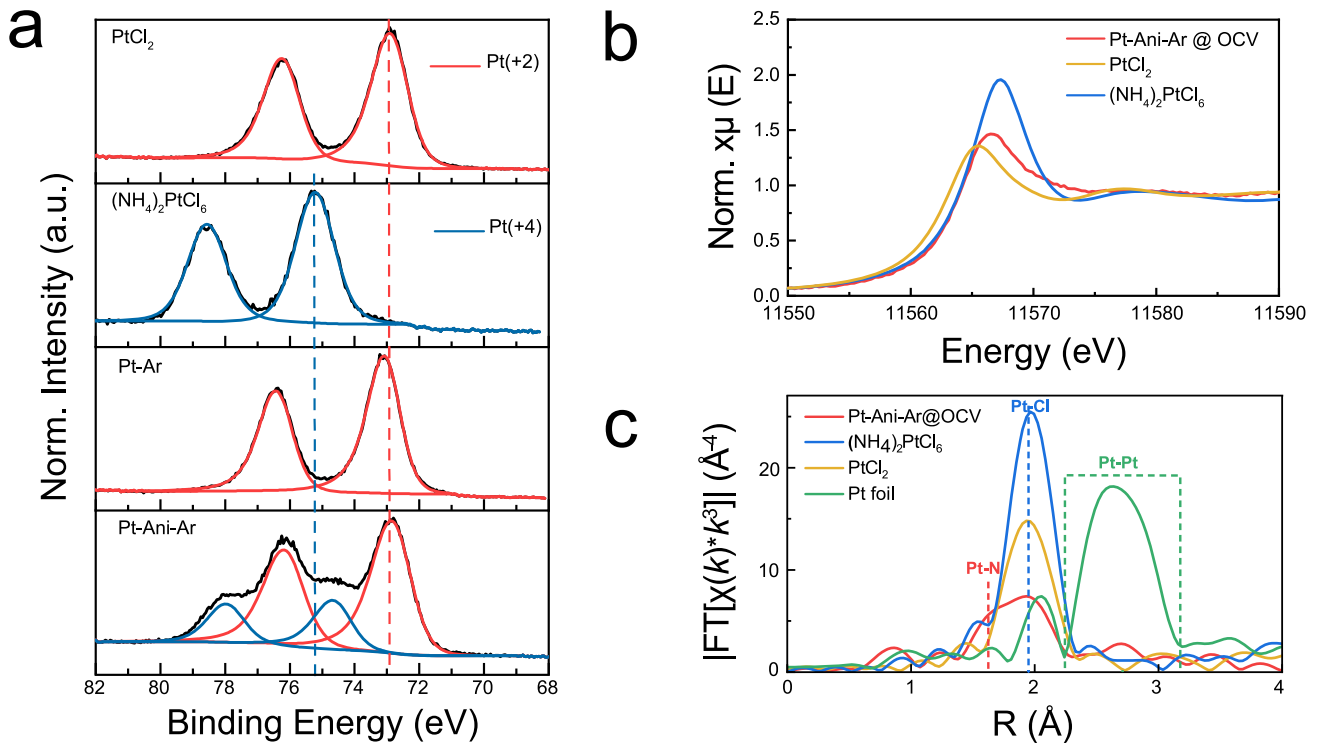

Figure 2. XPS spectra of Pt 4f (a) and XANES spectra (b) recorded at the Pt L_3 edge for the synthesized Pt SSC and control sample (Pt/Ar) compared with reference standards in oxidation states of platinum(II) and platinum(IV). Vertical dashed red and blue lines in a indicate the peak positions of $Pt_{7/2}$ at the oxidation state of platinum(II) and platinum(IV). (c) Corresponding k^3-weighted Fourier-transformed Pt L_3-edge EXAFS spectra of samples in b and standard Pt foil. Vertical dashed lines or area show the positions of Pt−N (red), Pt−Cl (blue), and Pt−Pt (green) peaks.

and Supplementary Figure S5b). These contributions likely arise from platinum(II) and platinum(IV),[36] respectively, indicating that the sample is a mixture of the two oxidation states.[24,25,37] (Pt/Ar) is well fitted by a single peak centered at 73.0 ± 0.1 eV arising from the +2 oxidation state (Supplementary Figure S6).[38,39] These oxidation-state assignments are consistent with the XANES spectra shown in Figure 2b. Here, reference spectra for $PtCl_2$ (+2) and $(NH_4)_2PtCl_6$ (+4) have white line peak positions at 11 565.8 and 11 567.7 eV, respectively. The spectrum for (Pt/Ani/Ar) has a single peak centered at 11 566.7 eV. This is expected of a mixture of platinum(II) and platinum(IV) and is consistent with the XPS data.[37,38]

The EXAFS spectra plotted in Figure 2c (along with those of the standards) give information about the platinum bonding environment. The standard samples of $PtCl_2$ and $(NH_4)_2PtCl_6$ have one dominant peak in the range from 1.5 to 2.3 Å with the center at 1.96 Å, suggesting that this peak can be associated with Pt−Cl bonding. The most intense peak in the spectrum for (Pt/Ani/Ar) is at 1.96 Å with a shoulder at 1.66 Å. The peak at 1.96 Å should arise from the presence of Pt−Cl bonds. This shoulder peak at 1.66 Å is indicative of platinum−nitrogen bonding.[40,41] Finally, there is the absence of obvious Pt−Pt bonding at 2.73 Å (green curve in Figure 2c), which also suggests that the platinum atoms are mainly isolated from each other. We therefore interpret these data to mean that the aniline and chloride coordinate to the platinum to form a complex molecule (Supplementary Figure S7).

These XPS and XANES data indicate that (Pt/Ani/Ar) and (Pt/Ar) are reduced in situ from platinum(IV) (the oxidation state of platinum in the precursor H_2PtCl_6) to platinum(II). The cause of the reduction of Pt(IV) to Pt(II) is the ethanol used as a solvent to prepare the H_2PtCl_6 solution (Supplementary Figure S8).[42] However, in (Pt/Ani/Ar), the platinum forms a complex with aniline (as confirmed by the bonding data from the EXAFS spectra). This is the reason that (Pt/Ani/Ar) is only partially reduced with platinum(IV) still present. The STEM, XPS, XANES, and EXAFS data suggest that the aniline-treated sample contains atomically dispersed platinum in the form of molecular complexes (Pt single-site complexes) physisorbed onto the graphene substrate.

Operando XAS Measurements. Operando hard XAS at the platinum L_3 edge was performed at different potentials to investigate the evolution of the platinum single-site complex's oxidation state and chemical bonding environment during the HER.[23,30,43] A customized three-electrode cell setup (Supplementary Figure S10) was mounted to investigate the aniline-treated sample (Pt/Ani/Ar). The chronoamperometric performance of (Pt/Ani/Ar) at various potentials is shown in Figure 3a (with an enlarged view shown in Figure 3b). The areal current densities are shown for at least 1000 s of operation at each of 10 voltages: 0.4, 0.3, 0.2, 0.1, 0.06, 0.02, 0, −0.02, −0.04, and −0.06 V versus the reversible hydrogen electrode (RHE). The open-circuit voltage (OCV) is 0.6 V versus RHE. None of the tests at a positive potential have an areal current density greater than 0.1 mA cm^{-2}. This is to be expected since the HER is only thermodynamically favorable below 0 V versus RHE. Indeed, the data for the test at 0 V show a minimal areal current density until about 600 s (out of approximately 1200 s in total) when the current jumps suddenly and then gradually increases to about −0.3 mA cm^{-2}. The areal current densities for the subsequent potentials of

https://doi.org/10.1021/acscatal.1c05958
ACS Catal. 2022, 12, 3173−3180

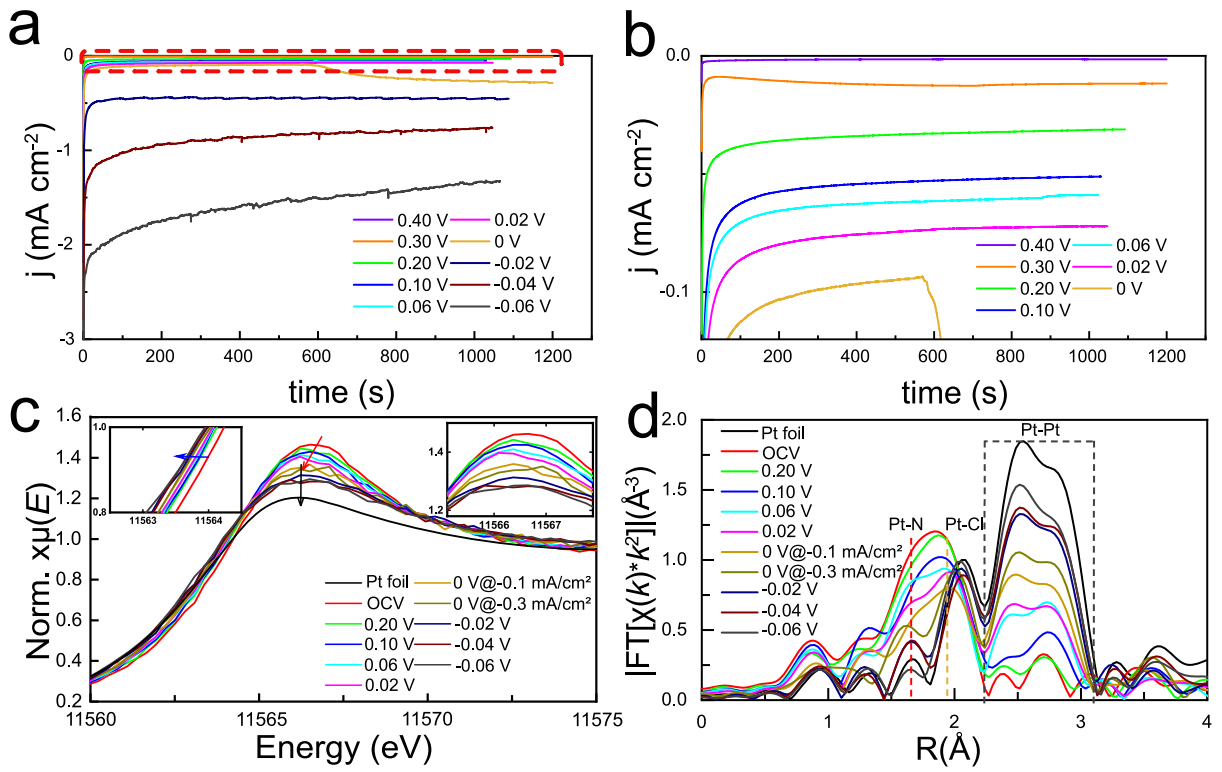

Figure 3. (a) Stable chronoamperometric curves of Pt single-site complex at various applied potentials. (b) Enlarged red dashed area in a shows the chronoamperometric curves at a current density smaller than 0.1 mA cm^{-2}. (c) Operando XANES spectra recorded at the Pt L_3 edge of the synthesized Pt single-site complex at different working potentials for the HER in 0.5 M H_2SO_4. (Insets) Energy shifts of the Pt L_3 absorption edge (left) and white-line peak (right). (d) Corresponding k^2-weighted Fourier-transformed EXAFS spectra (magnitude component). Vertical dashed lines or area show the Pt−N (red), Pt−Cl (orange), and Pt−Pt (gray) peaks.

−0.02, −0.04, and −0.06 V versus RHE are −0.5, −0.9, and −1.5 mA cm^{-2}, respectively. The Tafel slope, calculated using the 4 negative potentials, is 60 mV dec^{-1}. This is comparable to the Tafel slope of platinum nanoparticles for the HER.[44,45]

The average of eight XANES spectra, collected during operation at each potential, is shown in Figure 3c. These data show that the oxidation state of platinum decreases from a mixture of +4 and +2 to 0. When the potential is decreased from 0.6 (OCV) to 0 V versus RHE, the positions of both the white line (red arrow and right inset in Figure 3c) and the absorption edge (left inset in Figure 3c) in the XANES spectra show a negative shift of 0.4 eV. Those shifts suggest a continuous decrease of platinum valence from a mixture of platinum(II) and platinum(IV) to metallic platinum.[23,46]

The bonding environment of the platinum also changes as the applied potential varies, as shown in the EXAFS spectra in Figure 3d. As the potential is decreased from OCV to 0, the peaks at 1.66 and 1.96 Å, arising from Pt−N and Pt−Cl bonds, respectively, both decrease in intensity. However, the peak arising from Pt−N (blue vertical line) decreases faster than that arising from Pt−Cl (orange vertical line). This indicates that as the potential is decreased from OCV and while the oxidation state of the platinum falls to 0, the aniline molecules are dissociating from the complex. The chloride ions are also dissociating from the platinum atoms but to a lesser extent compared to the aniline molecules. At 0 V, the SSC has two distinct EXAFS spectra (yellow and olive curves in Figure 3d and isolated in Figure S12): one at a low areal current density (−0.1 mA cm^{-2}) before the onset of the HER and one at a higher areal current density (−0.3 mA cm^{-2}) after the onset of the HER. Before the onset of the HER, the bonding environment still shows appreciable Pt−Cl bonding and some Pt−N bonding. After 600 s and the beginning of hydrogen evolution, almost all Pt−N bonding character is lost and the Pt−Cl bonding feature decreases significantly. The EXAFS spectrum is instead dominated by Pt−Pt bonding. The rapid breaking of Pt−N and Pt−Cl bonds at 0 V may be caused by hydrogen molecules aggregated on the SSC. It has been experimentally shown that the diffusion and agglomeration of platinum atoms can be induced by exposure to a hydrogen atmosphere.[47−50] Since more reduced platinum structures after 600 s can boost the evolution of hydrogen by lowering the Gibbs free energy of hydrogen adsorption in acidic electrolytes,[23,51] the sudden increase in current density here (the yellowish line discussed in Figure 3a) can probably be justified accordingly.

Structure−Electrochemistry Correlation. The previous section elucidated the evolution of the Pt single-site complex into metallic nanoclusters at potentials below 0 V; the details of this transformation need to be quantitatively examined together with the catalytic activity. The effect of applied potential on both the areal current density and the platinum oxidation state in the SSC is shown in Figure 4a. The height of the XANES normalized white lines is summarized (black plot in Figure 4a) to quantify the evolution of platinum's oxidation state and the electron occupancy of platinum's 5d orbitals.[52,53] The white-line height decreases precipitously from OCV (0.60 V) to about 0 V versus RHE. This is consistent with the complete filling of the platinum 5d valence orbitals and the formation of metallic platinum.[23] At the same potential, the corresponding areal current density increases precipitously as the HER becomes thermodynamically favorable, although they

https://doi.org/10.1021/acscatal.1c05958
ACS Catal. 2022, 12, 3173−3180

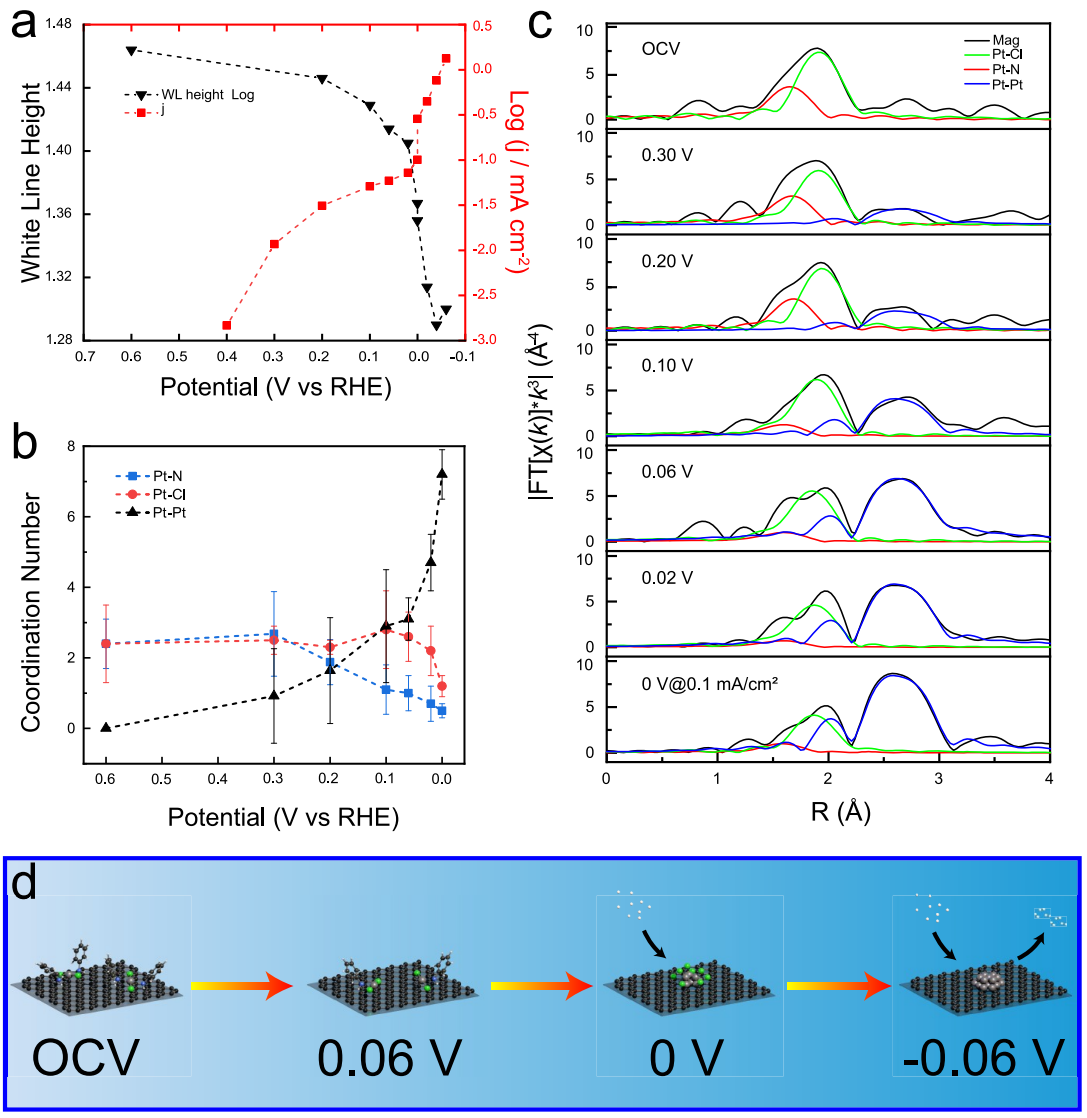

Figure 4. (a) Amplitude of the normalized white-line peak of the Pt L_3-edge operando XANES spectra (black) and corresponding catalytic activity (red) at different potentials. Log(j) is calculated using a relatively stable current density at the end of each CA test. (b) Coordination number of Pt−N, Pt−Cl, and Pt−Pt fitting paths for operando EXAFS data of the Pt single-site complex at selected potentials by 0 V. Error bars in b represent the uncertainties of the fitting results. (c) Contribution of different paths (Pt−N, Pt−Cl, and Pt−Pt) to fit the corresponding EXAFS spectra. Details of the fitting results shown in K-space and R-space are found in Figure S13. (d) Proposed schematic model for the evolution of the (Pt/Ani/Ar) sample from a single-site complex to subnanoclusters based on the operando EXAFS analysis (gray, Pt; green, Cl; blue, N; black, carbon; white, H).

are still relatively low (from −0.001 to −0.08 mA cm^{-2}). There is an obvious drop in white-line height at around 0 V, and the white-line height stabilizes at around 1.30 after 0 V, indicating the oxidation state of platinum remains as 0 at potentials below 0 V. Corresponding to the decrease in oxidation state, a significant increase in current density is also recorded at 0 V (red plot in Figure 4a).After the increase, a linear relationship between the base-10 logarithm of the areal current density and the potentials is presented.

EXAFS curve-fitting analysis on the platinum's EXAFS spectrum at OCV allows for the determination of a plausible molecular structure for the platinum complex adsorbed onto graphene. Considering eight possible platinum complexes described by $(C_6H_5NH_2)_xCl_yPt$ for x = 1 or 2 and y = 1, 2, 3, or 4, the Pt−N and Pt−Cl bond lengths (about 2.05 and 2.30 Å, respectively) determined by density-functional theory modeling of the isolated molecular complexes are the starting point for the analysis. The operando EXAFS data are best described by the structural model for *trans*-dianilinedichloroplatinum(II), $(C_6H_5NH_2)_2Cl_2Pt$(II), within the fitting range (k-range, 3−12.5 $Å^{-1}$, R-range, 1.1−2.5 Å, misfit factor 0.8%). This structure is consistent with the XPS and XANES spectra of the (Pt/Ani/Ar) sample (most of the Pt is at an oxidation of +2) and is similar to the previously reported crystal $(C_6H_5NH_2)_2PtCl_2$ complex prepared by mixing aniline with H_2PtCl_6.[54,55]

Performing EXAFS curve-fitting analysis (platinum's first (1.5−2.1 Å) and second (2.3−3.1 Å) coordination shells) on the spectra collected at different potentials results in the curves in Figure 4b and Table S1, which show the average number of platinum, chlorine, and nitrogen atoms coordinated to each platinum atom (i.e., the coordination number) as a function of applied potential. Specifically, Figure 4c highlights the evolution of the EXAFS spectra while decreasing potential in

https://doi.org/10.1021/acscatal.1c05958
ACS Catal. 2022, 12, 3173−3180

the *R* space fitted with the contributions of the Pt−N, Pt−Cl, and Pt−Pt paths. At OCV, the coordination number for both chlorine and nitrogen is about 2.5. As the potential is lowered, the coordination number for nitrogen decreases to about 1.0 by a potential of 0.1 V versus RHE. It continues to decrease to about 0.5 by 0 V (but before the onset of the HER). The chlorine coordination number stays higher than the nitrogen coordination number. This indicates that the aniline molecules dissociate from the complex before the chloride ions do, likely due to the more ionic character and higher bond energy of the Pt−Cl bonds compared to the Pt−N bonds.[56] The platinum coordination number increases as the potential is lowered, ultimately reaching a value of about 7.0 by 0 V versus RHE. This indicates the agglomeration of platinum as the potential is lowered (Supplementary Figure S14), which is also in line with the reduction of the oxidation state of platinum described in Figure 4a.[57]

Together these data elucidate how the platinum bonding environment in an SSC changes as a function of applied potential during operation, as described schematically in Figure 4d. As the potential is lowered from OCV, the dianilinedichloroplatinum(II) decomposes as the aniline dissociates from the platinum, followed by the dissociation of the chloride ions. Simultaneously, the 5d valence orbitals of platinum are filled. By the onset of the HER at 0 V versus RHE, the dianilinedichloroplatinum(II) complexes have completely dissociated and the metallic platinum(0) single atoms agglomerate into nanoclusters which catalyze the HER.

CONCLUSIONS

In this work, we use operando, synchrotron X-ray absorption spectroscopy to characterize how the oxidation state and bonding environment of platinum changes in an SSC for the HER at the molecular level. First, we show successful synthesis of a platinum SSC, confirming the platinum is atomically dispersed by STEM and XRD. We observe a mixture of platinum(II) and platinum(IV) by XPS and XANES, and we confirm platinum coordination to aniline by ex-situ EXAFS. We then probe the oxidation state and molecular structure as a function of applied potential using operando EXAFS and XANES with synchrontron radiation. We find that as the potential is lowered from OCV the platinum oxidation state decreases, breaking bonds between platinum atoms and aniline ligands first. The Pt−Cl bonds also break but to a lesser extent than the Pt−N bonds. Finally, once the onset of the HER at 0 V versus RHE is reached, the platinum is completely reduced and metallic platinum atoms agglomerate to form catalytic nanoclusters. Our work suggests that many single-site catalysts that achieve atomically dispersed platinum by ligand coordination do not remain atomically dispersed during device operation. This demonstrates that researchers should be extremely careful when assuming that the bonding environment of the as-synthesized SSC will remain the same during device operation. Furthermore, this operando study establishes two important structure−property relationships for aniline-complex platinum SSCs. First, platinum exists as metallic platinum (that is, in the oxidation state 0) while catalyzing the HER. Second, the molecular structure of the platinum complexes is lost due to the reduction of the platinum. These findings highlight the necessity for operando techniques to follow the dynamic behavior of SSCs during operation and provide critical new insight into why SSCs deactivate over time. Such experiments can also provide an important contribution to an atomic understanding of the structural evolution of SSC systems as well as SACs for other critical electrochemical reactions, such as the oxygen reduction reaction and carbon dioxide reduction reaction. These results and the operando X-ray spectroscopy method used in this study will accelerate the development of stable, high-performance platinum SSCs for clean hydrogen production.

ASSOCIATED CONTENT

Supporting Information

The Supporting Information is available free of charge at https://pubs.acs.org/doi/10.1021/acscatal.1c05958.

Experimental sections; additional STEM analysis and XPS data of (Pt/Ani/Ar) and (Pt/Ar); Raman spectra of (Pt/Ani/Ar); setup of the operando XAS experiment; details of EXAFS fitting results; STEM, XPS, and XAS of (Pt/Ani/Ar) sample post cycling (PDF)

AUTHOR INFORMATION

Corresponding Author

Mauro Pasta − *Department of Materials, University of Oxford, Oxford OX1 3PH, United Kingdom; Oxford Suzhou Centre for Advanced Research, Suzhou 215123 Jiangsu Province, P. R. China;* orcid.org/0000-0002-2613-4555; Email: mauro.pasta@materials.ox.ac.uk

Authors

Peng Tang − *Department of Materials, University of Oxford, Oxford OX1 3PH, United Kingdom*

Hyeon Jeong Lee − *Department of Materials, University of Oxford, Oxford OX1 3PH, United Kingdom*

Kevin Hurlbutt − *Department of Materials, University of Oxford, Oxford OX1 3PH, United Kingdom;* orcid.org/0000-0001-7494-0044

Po-Yuan Huang − *Department of Materials, University of Oxford, Oxford OX1 3PH, United Kingdom*

Sudarshan Narayanan − *Department of Materials, University of Oxford, Oxford OX1 3PH, United Kingdom*

Chenbo Wang − *Oxford Suzhou Centre for Advanced Research, Suzhou 215123 Jiangsu Province, P. R. China*

Diego Gianolio − *Diamond Light Source Limited, Harwell Science and Innovation Campus, Didcot, Oxfordshire OX11 0DE, United Kingdom;* orcid.org/0000-0002-0708-4492

Rosa Arrigo − *School of Science, Engineering and Environment, University of Salford, Manchester M5 4WT, United Kingdom*

Jun Chen − *Department of Materials, University of Oxford, Oxford OX1 3PH, United Kingdom*

Jamie H. Warner − *Materials Graduate Program, Texas Materials Institute, The University of Texas at Austin, Austin, Texas 78712, United States; Walker Department of Mechanical Engineering, The University of Texas at Austin, Austin, Texas 78712, United States*

Complete contact information is available at: https://pubs.acs.org/10.1021/acscatal.1c05958

Author Contributions

P.T. and M.P. conceived and designed the experiments. P.T. prepared the samples and performed the electrochemical tests. P.T., J.C., and J.H.W. performed the aberration-corrected STEM characterization and analyzed the data. D.G. and R.A. conducted the operando XAFS experiments at Diamond Light

https://doi.org/10.1021/acscatal.1c05958
ACS Catal. 2022, 12, 3173−3180

Source under the proposal of SP_26066. P.T. and H.J.L. analyzed the operando XAFS data. P.-Y.H. and P.T. prepared the reference samples and calibrated the three-electrode cell used in the operando XAFS study. S.N. performed the XPS characterization and contributed to XPS data interpretation. K.H. conducted the DFT calculations. P.T., K.H., and C.W. wrote the manuscript with input from all authors. M.P. supervised the design of the project and gave frequent, in-depth scientific input.

Notes

The authors declare no competing financial interest.

Source data are available from the corresponding author upon reasonable request.

■ ACKNOWLEDGMENTS

We acknowledge the financial support of the Jiangsu Industrial Technology Research Institute (JITRI) and the Henry Royce Institute (through UK Engineering and Physical Science Research Council grant EP/R010145/1) for capital equipment. We acknowledge Diamond Light Source for time on B18 Beamline under Proposal SP-26066. We are grateful to the David Cockayne Centre for Electron Microscopy for the use of their electron microscopes.

■ REFERENCES

(1) *Hydrogen From Renewable Power: Technology outlook for the energy transition*; IRENA, 2018.

(2) Lagadec, M. F.; Grimaud, A. Water electrolysers with closed and open electrochemical systems. *Nat. Mater.* **2020**, *19*, 1140−1150.

(3) McCrory, C. C.; Jung, S.; Ferrer, I. M.; Chatman, S. M.; Peters, J. C.; Jaramillo, T. F. Benchmarking hydrogen evolving reaction and oxygen evolving reaction electrocatalysts for solar water splitting devices. *J. Am. Chem. Soc.* **2015**, *137*, 4347−4357.

(4) Cui, X.; Li, W.; Ryabchuk, P.; Junge, K.; Beller, M. Bridging homogeneous and heterogeneous catalysis by heterogeneous single-metal-site catalysts. *Nature Catalysis* **2018**, *1*, 385−397.

(5) Kibsgaard, J.; Chorkendorff, I. Considerations for the scaling-up of water splitting catalysts. *Nature Energy* **2019**, *4*, 430−433.

(6) Thomas, J. M.; Raja, R.; Lewis, D. W. Single-site heterogeneous catalysts. *Angew. Chem., Int. Ed.* **2005**, *44*, 6456−6482.

(7) Pelletier, J. D.; Basset, J.-M. Catalysis by design: well-defined single-site heterogeneous catalysts. *Accounts of chemical research* **2016**, *49*, 664−677.

(8) Thomas, J. M. The concept, reality and utility of single-site heterogeneous catalysts (SSHCs). *Phys. Chem. Chem. Phys.* **2014**, *16*, 7647−7661.

(9) Li, Z.; Wang, D.; Wu, Y.; Li, Y. Recent advances in the precise control of isolated single-site catalysts by chemical methods. *National Science Review* **2018**, *5*, 673−689.

(10) Ye, S.; Luo, F.; Zhang, Q.; Zhang, P.; Xu, T.; Wang, Q.; He, D.; Guo, L.; Zhang, Y.; He, C. Highly stable single Pt atomic sites anchored on aniline-stacked graphene for hydrogen evolution reaction. *Energy Environ. Sci.* **2019**, *12*, 1000−1007.

(11) Li, C.; Chen, Z.; Yi, H.; Cao, Y.; Du, L.; Hu, Y.; Kong, F.; Kramer Campen, R.; Gao, Y.; Du, C.; et al. Polyvinylpyrrolidone-Coordinated Single-Site Platinum Catalyst Exhibits High Activity for Hydrogen Evolution Reaction. *Angew. Chem., Int. Ed.* **2020**, *59*, 15902−15907.

(12) Chen, Y.; Ji, S.; Chen, C.; Peng, Q.; Wang, D.; Li, Y. Single-atom catalysts: synthetic strategies and electrochemical applications. *Joule* **2018**, *2*, 1242−1264.

(13) Yang, X.-F.; Wang, A.; Qiao, B.; Li, J.; Liu, J.; Zhang, T. Single-atom catalysts: a new frontier in heterogeneous catalysis. *Accounts of chemical research* **2013**, *46*, 1740−1748.

(14) Wang, A.; Li, J.; Zhang, T. Heterogeneous single-atom catalysis. *Nature Reviews Chemistry* **2018**, *2*, 65−81.

(15) Zhang, J.; Zhao, Y.; Guo, X.; Chen, C.; Dong, C.-L.; Liu, R.-S.; Han, C.-P.; Li, Y.; Gogotsi, Y.; Wang, G. Single platinum atoms immobilized on an MXene as an efficient catalyst for the hydrogen evolution reaction. *Nature Catalysis* **2018**, *1*, 985−992.

(16) Tang, C.; Chen, L.; Li, H.; Li, L.; Jiao, Y.; Zheng, Y.; Xu, H.; Davey, K.; Qiao, S.-Z. Tailoring Acidic Oxygen Reduction Selectivity on Single-Atom Catalysts via Modification of First and Second Coordination Spheres. *J. Am. Chem. Soc.* **2021**, *143*, 7819−7827.

(17) Pang, J.; Chang, B.; Liu, H.; Zhou, W. Potential of MXene-Based Heterostructures for Energy Conversion and Storage. *ACS Energy Letters* **2022**, *7*, 78−96.

(18) Mitchell, S.; Vorobyeva, E.; Pérez-Ramírez, J. The multifaceted reactivity of single-atom heterogeneous catalysts. *Angew. Chem., Int. Ed.* **2018**, *57*, 15316−15329.

(19) Copéret, C. Single-sites and nanoparticles at tailored interfaces prepared via surface organometallic chemistry from thermolytic molecular precursors. *Accounts of chemical research* **2019**, *52*, 1697−1708.

(20) Zhao, D.; Zhuang, Z.; Cao, X.; Zhang, C.; Peng, Q.; Chen, C.; Li, Y. Atomic site electrocatalysts for water splitting, oxygen reduction and selective oxidation. *Chem. Soc. Rev.* **2020**, *49*, 2215−2264.

(21) Zhao, S.; Yang, Y.; Tang, Z. Insight into Structural Evolution, Active Sites, and Stability of Heterogeneous Electrocatalysts. *Angew. Chem., Int. Ed.* **2022**, No. e202110186.

(22) Li, X.; Yang, X.; Zhang, J.; Huang, Y.; Liu, B. In Situ/Operando techniques for characterization of single-atom catalysts. *ACS Catal.* **2019**, *9*, 2521−2531.

(23) Fang, S.; Zhu, X.; Liu, X.; Gu, J.; Liu, W.; Wang, D.; Zhang, W.; Lin, Y.; Lu, J.; Wei, S.; et al. Uncovering near-free platinum single-atom dynamics during electrochemical hydrogen evolution reaction. *Nat. Commun.* **2020**, *11*, 1029.

(24) Kaiser, S. K.; Fako, E.; Manzocchi, G.; Krumeich, F.; Hauert, R.; Clark, A. H.; Safonova, O. V.; López, N.; Pérez-Ramírez, J. Nanostructuring unlocks high performance of platinum single-atom catalysts for stable vinyl chloride production. *Nature Catalysis* **2020**, *3*, 376−385.

(25) Ren, Y.; Tang, Y.; Zhang, L.; Liu, X.; Li, L.; Miao, S.; Sheng Su, D.; Wang, A.; Li, J.; Zhang, T. Unraveling the coordination structure-performance relationship in Pt_1/Fe_2O_3 single-atom catalyst. *Nat. Commun.* **2019**, *10*, 4500.

(26) Huebner, S.; de Vries, J. G.; Farina, V. Why does industry not use immobilized transition metal complexes as catalysts? *Advanced Synthesis & Catalysis* **2016**, *358*, 3−25.

(27) Timoshenko, J.; Roldan Cuenya, B. In situ/operando electrocatalyst characterization by X-ray absorption spectroscopy. *Chem. Rev.* **2021**, *121*, 882−961.

(28) Malta, G.; Kondrat, S. A.; Freakley, S. J.; Davies, C. J.; Dawson, S.; Liu, X.; Lu, L.; Dymkowski, K.; Fernandez-Alonso, F.; Mukhopadhyay, S.; et al. Deactivation of a single-site gold-on-carbon acetylene hydrochlorination catalyst: an X-ray absorption and inelastic neutron scattering study. *ACS Catal.* **2018**, *8*, 8493−8505.

(29) Liu, L.; Meira, D. M.; Arenal, R.; Concepcion, P.; Puga, A. V.; Corma, A. Determination of the evolution of heterogeneous single metal atoms and nanoclusters under reaction conditions: which are the working catalytic sites? *ACS catalysis* **2019**, *9*, 10626−10639.

(30) Maurer, F.; Jelic, J.; Wang, J.; Gänzler, A.; Dolcet, P.; Wöll, C.; Wang, Y.; Studt, F.; Casapu, M.; Grunwaldt, J. D. Tracking the formation, fate and consequence for catalytic activity of Pt single sites on CeO_2. *Nature Catalysis* **2020**, *3*, 824−833.

(31) Fei, H.; Dong, J.; Chen, D.; Hu, T.; Duan, X.; Shakir, I.; Huang, Y.; Duan, X. Single atom electrocatalysts supported on graphene or graphene-like carbons. *Chem. Soc. Rev.* **2019**, *48*, 5207−5241.

(32) Lee, J. K.; Bulut, I.; Rickhaus, M.; Sheng, Y.; Li, X.; Han, G. G.; Briggs, G. A. D.; Anderson, H. L.; Warner, J. H. Metal atom markers for imaging epitaxial molecular self-assembly on graphene by scanning transmission electron microscopy. *ACS Nano* **2019**, *13*, 7252−7260.

(33) Li, Y.; Zhou, W.; Wang, H.; Xie, L.; Liang, Y.; Wei, F.; Idrobo, J. C.; Pennycook, S. J.; Dai, H. An oxygen reduction electrocatalyst

https://doi.org/10.1021/acscatal.1c05958
ACS Catal. 2022, 12, 3173−3180

based on carbon nanotube-graphene complexes. *Nat. Nanotechnol.* **2012**, *7*, 394−400.
(34) Li, X.; Lee, J. K.; Lu, Y.; Gerkman, M. A.; Kengmana, E. S.; Fonseca, M. V.; Warner, J. H.; Han, G. G. Precursor design for high density single Pt atom sites on MoS2: enhanced stability at elevated temperatures and reduced 3D clustering. *Chem. Mater.* **2020**, *32*, 2541−2551.
(35) Shiell, T. B.; de Tomas, C.; McCulloch, D. G.; McKenzie, D. R.; Basu, A.; Suarez-Martinez, I.; Marks, N.; Boehler, R.; Haberl, B.; Bradby, J. In situ analysis of the structural transformation of glassy carbon under compression at room temperature. *Phys. Rev. B* **2019**, *99*, 024114.
(36) Yang, M.; Liu, J.; Lee, S.; Zugic, B.; Huang, J.; Allard, L. F.; Flytzani-Stephanopoulos, M. A common single-site Pt(II)-O(OH)x-species stabilized by sodium on "active" and "inert" supports catalyzes the water-gas shift reaction. *J. Am. Chem. Soc.* **2015**, *137*, 3470−3473.
(37) Liu, J.; Jiao, M.; Lu, L.; Barkholtz, H. M.; Li, Y.; Wang, Y.; Jiang, L.; Wu, Z.; Liu, D.- j.; Zhuang, L.; et al. High performance platinum single atom electrocatalyst for oxygen reduction reaction. *Nat. Commun.* **2017**, *8*, 15938.
(38) Cheng, X.; Li, Y.; Zheng, L.; Yan, Y.; Zhang, Y.; Chen, G.; Sun, S.; Zhang, J. Highly active, stable oxidized platinum clusters as electrocatalysts for the hydrogen evolution reaction. *Energy Environ. Sci.* **2017**, *10*, 2450−2458.
(39) Imaoka, T.; Akanuma, Y.; Haruta, N.; Tsuchiya, S.; Ishihara, K.; Okayasu, T.; Chun, W. J.; Takahashi, M.; Yamamoto, K. Platinum clusters with precise numbers of atoms for preparative-scale catalysis. *Nat. Commun.* **2017**, *8*, 688.
(40) Lim, T.; Jung, G. Y.; Kim, J. H.; Park, S. O.; Park, J.; Kim, Y. T.; Kang, S. J.; Jeong, H. Y.; Kwak, S. K.; Joo, S. H. Atomically dispersed Pt-N_4 sites as efficient and selective electrocatalysts for the chlorine evolution reaction. *Nat. Commun.* **2020**, *11*, 412.
(41) Li, X.; Bi, W.; Zhang, L.; Tao, S.; Chu, W.; Zhang, Q.; Luo, Y.; Wu, C.; Xie, Y. Single-atom Pt as co-catalyst for enhanced photocatalytic H_2 evolution. *Adv. Mater.* **2016**, *28*, 2427−2431.
(42) Obreja, L.; Foca, N.; Popa, M.; Melnig, V. Alcoholic reduction platinum nanoparticles synthesis by sonochemical method. *Biomater. Biophys., Med. Phys. Ecol.* **2008**, .3136
(43) Wang, J.; Tan, H.-Y.; Kuo, T.-R.; Lin, S.-C.; Hsu, C.-S.; Zhu, Y.; Chu, Y.-C.; Chen, T. L.; Lee, J.-F.; Chen, H. M. In Situ identifying the dynamic structure behind activity of atomically dispersed Platinum catalyst toward hydrogen evolution reaction. *Small* **2021**, *17*, 2005713.
(44) Ghanim, A. H.; Koonce, J. G.; Hasa, B.; Rassoolkhani, A. M.; Cheng, W.; Peate, D. W.; Lee, J.; Mubeen, S. Low-loading of Pt nanoparticles on 3D carbon foam support for highly active and stable hydrogen production. *Front. Chem.* **2018**, *6*, 523.
(45) Kang, J.; Wang, M.; Lu, C.; Ke, C.; Liu, P.; Zhu, J.; Qiu, F.; Zhuang, X. Platinum Atoms and Nanoparticles Embedded Porous Carbons for Hydrogen Evolution Reaction. *Materials* **2020**, *13*, 1513.
(46) Mansour, A.; Cook, J., Jr; Sayers, D. Quantitative technique for the determination of the number of unoccupied d-electron states in a platinum catalyst using the $L_{2,3}$ X-ray absorption edge spectra. *J. Phys. Chem.* **1984**, *88*, 2330−2334.
(47) Horch, S.; Lorensen, H. T.; Helveg, S.; Lægsgaard, E.; Stensgaard, I.; Jacobsen, K. W.; Nørskov, J. K.; Besenbacher, F. Enhancement of surface self-disfusion of platinum atoms by adsorbed hydrogen. *Nature* **1999**, *398*, 134−136.
(48) Parkinson, G. S.; Novotny, Z.; Argentero, G.; Schmid, M.; Pavelec, J.; Kosak, R.; Blaha, P.; Diebold, U. Carbon monoxide-induced adatom sintering in a Pd-Fe_3O_4 model catalyst. *Nat. Mater.* **2013**, *12*, 724−728.
(49) Dessal, C.; Sangnier, A.; Chizallet, C.; Dujardin, C.; Morfin, F.; Rousset, J. L.; Aouine, M.; Bugnet, M.; Afanasiev, P.; Piccolo, L. Atmosphere-dependent stability and mobility of catalytic Pt single atoms and clusters on γ-Al_2O_3. *Nanoscale* **2019**, *11*, 6897−6904.
(50) Liu, L.; Lopez-Haro, M.; Meira, D. M.; Concepcion, P.; Calvino, J. J.; Corma, A. Regioselective Generation of Single-Site Iridium Atoms and Their Evolution into Stabilized Subnanometric Iridium Clusters in MWW Zeolite. *Angew. Chem., Int. Ed.* **2020**, *59*, 15695−15702.
(51) Shi, Y.; Ma, Z.-R.; Xiao, Y.-Y.; Yin, Y.-C.; Huang, W.-M.; Huang, Z.-C.; Zheng, Y.-Z.; Mu, F.-Y.; Huang, R.; Shi, G.-Y.; et al. Electronic metal-support interaction modulates single-atom platinum catalysis for hydrogen evolution reaction. *Nat. Commun.* **2021**, *12*, 3021.
(52) Wang, J.; et al. Redirecting dynamic surface restructuring of a layered transition metal oxide catalyst for superior water oxidation. *Nature Catalysis* **2021**, *4*, 212−222.
(53) Malta, G.; Kondrat, S. A.; Freakley, S. J.; Davies, C. J.; Lu, L.; Dawson, S.; Thetford, A.; Gibson, E. K.; Morgan, D. J.; Jones, W.; Wells, P. P.; Johnston, P.; Catlow, C. R. A.; Kiely, C. J.; Hutchings, G. J. Identification of single-site gold catalysis in acetylene hydrochlorination. *Science* **2017**, *355*, 1399−1403.
(54) Mohanraju, K.; Lee, H.; Kwon, O. J. High loading Pt core/carbon shell derived from platinum-aniline complex for direct methanol fuel cell application. *Electroanalysis* **2018**, *30*, 1604−1609.
(55) Kong, P.-C.; Rochon, F. Cis- and trans-platinum complexes of anilines. A study of isormerization reactions. *Inorg. Chim. Acta* **1982**, *61*, 269−271.
(56) Astakhov, A.; Soliev, S.; Chernyshev, V. Metal-ligand bond dissociation energies in the Ni, Pd, and Pt complexes with N-heterocyclic carbenes: effect of the oxidation state of the metal (0,+2). *Russian Chemical Bulletin* **2020**, *69*, 2073−2081.
(57) Hao, X.; Zhu, N.; Gschneidtner, T.; Jonsson, E. Ö.; Zhang, J.; Moth-Poulsen, K.; Wang, H.; Thygesen, K. S.; Jacobsen, K. W.; Ulstrup, J.; et al. Direct measurement and modulation of single-molecule coordinative bonding forces in a transition metal complex. *Nat. Commun.* **2013**, *4*, 2121.

https://doi.org/10.1021/acscatal.1c05958
ACS Catal. 2022, 12, 3173−3180